band, approximately as $L_x \sim 10^{-26.8}\ n_t^2\ T_t^{1/2}\ V_t$ erg s^{-1}, where V_t is the effective volume of the emitting region, $\sim r_v^3$. In the preceding example $r_v \sim 10^{10.9}$ cm and $L_x \sim 10^{33}$ erg s^{-1}. The kinetic energy flux in the flow at r_v is $EA \sim 10^{33.5}$ erg s^{-1} so that the required energy can be supplied.

Such a system can naturally and simultaneously possess an optically thick, more energetic, pulsed X-ray source, derived from the ultimate accretion of the material (parallel to field lines) onto the magnetic poles of the central object.

We note that the non-steady state can also be of interest. So long as some material is being accreted from infinity it should accumulate in the throat region (held out by the waves produced by the rotating central object) until the density for steady accretion, n_t, is reached there. The region will then empty onto the star, and the process should repeat. This would produce periodic X-ray flaring with period $P \sim \rho_t r_v^3\ (A_t + A_B)/(A_B\ A_t)$ or $\sim(\Phi^2/(4\pi)^2)\rho_\infty^{-1} C_\infty^3 (GM)^{-3}$ when $A_t \gg A_B$ (A_t is the magnetic accretion rate from the throat).

Using the illustrative values of Φ, M we have $P \sim 10^3\ T_\infty^{3/2}\ n_\infty^{-1}$ (~ 1 yr for typical interstellar medium parameters). The duty cycle would be roughly $A_B/A_t \sim 10^6\ n_\infty\ T_\infty^{-3/2}\ n_t^{-1/2}$, so that the "on time" is just $10^9\ n_t^{-1/2}$ s. This is at most a few days in these cases (one expects really a gradual strengthening over about a year followed by a rapid decline from maximum). This mechanism may be relevant to variable galactic sources.

Such systems may already have been observed in CX-3 and HX-1 (refs. 9, 10). But the binary nature of these sources may introduce complications. We do not expect our theory to apply exactly unless the orbital velocity of the central object is less than $v_\phi\ (r_v)$. Moreover, the likely presence of gas streams in the system will present a changing supply of accretable material. It is possible that such orbiting material may permit an explanation of the observed anomalous minima if the orbit were comet-like (to pass through such a cloud in about 9 days at a speed of a few hundred km s^{-1} (ref. 10) requires the cloud size (and thus the orbit size) to be $\gtrsim 10^{13}$ cm). But if this is so, one should observe the strong optically thin emission appearing and decaying before the strong pulsed emission (assuming the encounter does not always coincide with an eclipse) by a time at least of order r_v/w ($\sim 10^{3.2}$ s in the above example, and about 10^2 s for CX-3 as discussed below).

Applying the theory as it stands, however, we find from the energy suggested[9] for CX-3 (10^{35} erg s^{-1} in nonpulsed emission) that $n_t \lesssim 10^{14}$ cm^{-3}, $v_\phi^* \lesssim 10^8$ cm s^{-1}, $r_v \sim 10^{10.1}$ cm and $A \sim 10^{18.7}$ g s^{-1} sr^{-1}. One can check that EA again exceeds the radiated energy (in a unit solid angle). The required density of the cloud region is $n_\infty \sim 10^6$ cm^{-3} so that $T_t \sim 10^{6.5}$ K (again taking $\gamma \sim 1.4$. The temperature is unfortunately quite sensitive to γ. For $\gamma \sim 1.6$, $T_t \sim 10^8$ K).

If we take the asymptotic behaviour of v_ϕ for $r \ll r_v$, namely[7] $v_\phi \propto r^{1/2}$ as holding everywhere inside r_v, then with the above value of $v_\phi\ (r_v)$ we have $\Omega r_* \simeq 10^8 (r_x/r_y)^{1/2}$ or $r_x \sim 5 \times 10^5$ cm with $2\pi/\Omega = 4.84$ s. This is a lower limit to r_* because v_ϕ will not vary so rapidly as assumed near r_v, but it suggests that CX-3 is a neutron star rather than a white dwarf.

In HX-1 an interpulse seems to have been observed[10]. We expect these on the present model because of the probable thermal origin of the pulsed emission. If we assume a simple geometry, then the inclination between the rotation and magnetic axis is $\chi = \pi/2 - (\theta_1 + \theta_2)/2$, where θ_1, θ_2 are the angles made by the line of sight to the two magnetic poles (θ_1 is the smaller; that is, refers to brighter pole). If we assume that the observed intensity ratio[10] (pulse-interpulse) of about 2 is simply a projection effect (cosine ratio), and for θ_2, within 20° of 0°, $\theta_2 \sim 60°$ and $\chi \sim 50°$–60°. To make the intensity ratio at least to 10 to 1 as may be true for CX-3 we find $\chi \sim 38°$–48° for θ_1 within 20° of 0°.

The numbers given here are primarily qualitative; but it is intriguing to observe how closely this new picture has duplicated the numerical results of Prendergast and Burbidge[11], who worked from the observed properties of SX-1 and CX-2 but allowed also for the effects of angular momentum.

This research was supported in part by the National Research Council of Canada. One of us (R. N. H.) acknowledges the support of the Alexander von Humboldt Foundation and thanks Dr J. Trümper for a stimulating conversation.

R. N. HENRIKSEN *
T. T. CHIA

Astronomy Group, Department of Physics, Queen's University at Kingston, Ontario

Received August 22, 1972.

* Present address: Astronomisches Institut der Universität Tübingen, 74 Tübingen.

1 Bondi, H., *Mon. Not. Roy. Astron. Soc.*, **112**, 195 (1962).
2 McCrea, W. H., *Astrophys. J.*, **124**, 461 (1956).
3 Mestel, L., *Mon. Not. Roy. Astron. Soc.*, **119**, 223 (1959).
4 Havnes, O., and Conti, P. W., *Astron. Astrophys.*, **14**, 1 (1971).
5 Ostriker, J. P., Rees, M. J., and Silk, J., *Astrophys. Lett.*, **6**, 79 (1970).
6 Margon, B., Bowyer, S., Lampton, M., and Cruddace, R., *Astrophys. J. Lett.*, **169**, L 45 (1971).
7 Chia, T. T., and Henriksen, R. N., *Astrophys. J.*, **177** (in the press).
8 Henriksen, R. N., *Phys. of Fluids*, **13**, 353 (1970).
9 Schreier, E., Levinson, R., Gursky, H., Kellogg, E., Tananbaum, H., and Giacconi, R., *Astrophys. J. Lett.*, **172**, L 79 (1972).
10 Tananbaum, H., Gursky, H., Kellogg, E. M., Levinson, R., Schreier, E., and Giacconi, R., *Astrophys. J. Lett.*, **174**, L 143 (1972).
11 Prendergast, K. H., and Burbidge, G. R., *Astrophys. J. Lett.*, **151**, L 83 (1968).

Rigidity Spectrum of Helium Nuclei above 17 GV and a Search for High Energy Anti-nuclei in Primary Cosmic Rays

WE present here some results obtained with a magnet spectrograph flown from Hyderabad (geomagnetic cutoff ~ 17 GV) in May 1970. The two principal results are: there is no anomaly in the differential spectrum of helium nuclei close to the geomagnetic cutoff; and no anti-nuclei have been seen up to a rigidity of ~ 100 GV.

The instrument has been described earlier[1]. It consists basically of three glass plates covered with emulsion for accurate coordinate measurement, a 2 kG permanent magnet for particle bending, two wide gap spark chambers for trajectory location and a suitable triggering system. A total of 116 nuclei (mostly helium and some heavier) have been followed from spark chambers to the nearest emulsion plate and subsequently to other plates. The procedures for track-following and other questions, such as the errors involved, are discussed elsewhere[2].

The coordinates of the tracks in the three plates were measured to an accuracy of ~ 1 μm. The surfaces of the glass plates were optically worked and calibrated such that their profile was known to an accuracy of ~ 2 μm. The total error in the determination of the sagitta of the trajectory in the middle plate was ~ 3 μm. Mean sagitta of a 15 GV particle being 45 μm, the maximum detectable rigidity was ~ 220 GV. The error due to multiple Coulomb scattering (chiefly in the central plate) was $\sim 27\%$.

A common coordinate frame for the three plates can be obtained by demanding the linearity of field-free tracks. Because these were not available, we had to devise a procedure for using the tracks passing through the magnetic aperture, making use of the fact that these tracks differ from the field-free tracks only through a bending in a well defined direction. Measurements of these tracks, then, yield a deflexion distribution whose zero is shifted from that of the true distribution by an unknown amount. By changing the zero offset of this distribution one obtains varying rigidity distributions. But if

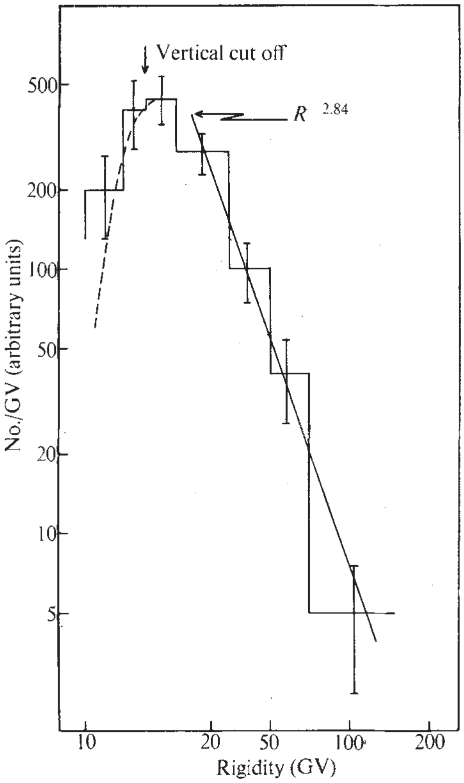

Fig. 1 Differential rigidity spectrum of helium nuclei. The smooth line is the power law fit to the spectrum beyond 22 GV. The broken line is the spectrum below 22 GV calculated on the basis of the directional variation of geomagnetic cutoff and the multiple Coulomb scattering.

above a certain rigidity (20 GV) the true distribution is assumed to be a power law in rigidity, then it becomes possible to fix the position of the zero point on the deflexion scale, and hence also the exponent of the power law, by demanding that the expected and observed deflexion distributions match each other. The requirement of a good match even at the tail, extending a little way (up to $1/R = -0.015\ GV^{-1}$) into the negative side, derives from the tacit assumption that this tail is entirely due to the spillover of particles from the positive side.

We emphasize that we do not have any negative rigidity below 60 GV even if the zero offset corresponded to a spectrum as flat as that with a differential exponent of -2.0; for a steeper spectrum, say, with an exponent -2.6, there is no negative particle with rigidity less than 100 GV.

The final rigidity spectrum thus derived is shown in Fig. 1. Because we are accepting tracks up to 30° from the vertical, we do not have a sharp geomagnetic cutoff; instead it varies from 14 to 22 GV depending on the direction. Also the shape of the spectrum near cutoff is smeared owing to Coulomb scattering. The expected shape was calculated taking into account the directional variation of the geomagnetic cutoff[3] and the Coulomb scattering distribution. This is shown by the broken lines in Fig. 1 and is seen to be quite consistent with the observed spectrum. Thus we do not find any evidence for a deficiency of particles near the geomagnetic cutoff as was observed by Golden *et al.*[4] for their measurements of heavy ($Z > 2$) particles over Texas (vertical cutoff 4.5 GV). If an effect similar to that observed by Golden *et al.*[4] existed for us, we would have expected 20 particles below 25 GV in place of 52 which are actually observed; in the absence of any such anomaly the expected number is 47. The differential slope fitted to the spectrum in the range 22–150 GV is 2.8 ± 0.15.

In Fig. 2 we have collected various measurements, including our present results, on the differential rigidity spectrum of helium nuclei beyond 10 GV. Our spectrum is normalized to accord with the integral flux of helium nuclei at Hyderabad measured by Anand *et al.*[5]. Also the integral measurements of Pinkau *et al.*[6] and Grigorov *et al.*[7] have been converted into differential points. The measurements shown in the figure have been made by one of the two techniques: magnetic bending or ionization calorimetry. The two sets of measurement agree with each other rather well in the overlapping region. The spectrum is quite smooth up to the highest energy of ~2,000 GV and consistent with a slope of -2.7.

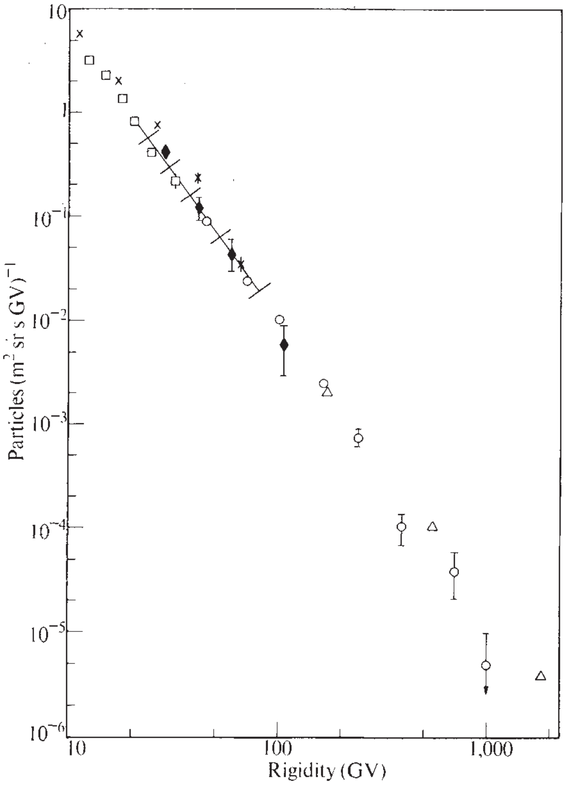

Fig. 2 Differential rigidity spectrum of the helium nuclei for rigidity higher than 10 GV as measured in various experiments. Data points for measurements of Pinkau *et al.*[6] and Grigorov *et al.*[7] have been derived from the integral values given by them. □, Anand *et al.*[5] (geomagnetic effect); ×, Buffington *et al.*[8] (magnet spectrograph); ◆, present experiment (magnet spectrograph); ○, Ryan *et al.*[9] (calorimeter); △, Grigorov *et al.*[7] (calorimeter); ++++, Pinkau *et al.*[6] (calorimeter).

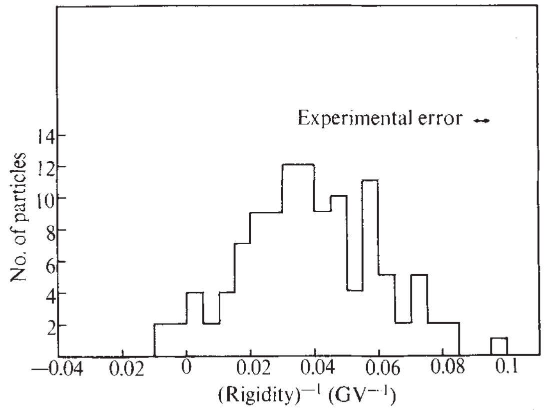

Fig. 3 Inverse-rigidity distribution for all the measured tracks. It is seen that there is no negative value beyond $-0.01\ (GV)^{-1}$. The experimental error is about $0.005\ (GV)^{-1}$.

Because in this experiment we measure the deflexion of particles in a magnetic field we would directly see anti-nuclei if they were present. In Fig. 3 we have plotted the measured $1/R$ spectrum for the exponent of the rigidity spectrum -2.8. The total measurement error is about $0.005\ (GV)^{-1}$. There are

Table 1 Results of Various Searches for Anti-nuclei in Cosmic Rays

Nuclear species	Rigidity/energy range	Fractional upper limit to anti-nuclei	Reference
Protons	100–150 MeV	3×10^{-4}	Apparao[10]
Protons	2.3–5.3 GeV	5×10^{-3}	Bogomolov *et al.*[11]
$Z\geq2$	200–800 MeV/N	10^{-3}	Aizu *et al.*[15]
Helium	0.3–3 GeV/N	10^{-2}	Evenson and Meyer[12]
$Z\geq2$	5–33 GV	3×10^{-4}	Buffington *et al.*[13]
$Z\geq2$	33–100 GV	2×10^{-2}	Buffington *et al.*[13]
$Z\geq3$	5–100 GV	1.4×10^{-2}	Golden *et al.*[4]
$Z\geq3$	5–20 GV	2.6×10^{-2}	Golden *et al.*[4]
$Z\geq3$	20–60 GV	9×10^{-2}	Golden *et al.*[4]
$Z\geq3$	60–125 GV	4×10^{-1}	Golden *et al.*[4]
$Z\geq2$	14–100 GV	10^{-2}	Present experiment
$Z\geq2$	14–30 GV	2×10^{-2}	Present experiment
$Z\geq2$	30–50 GV	2×10^{-2}	Present experiment
$Z\geq2$	50–100 GV	10^{-1}	Present experiment
$Z\geq6$	5–9 GeV/N	7.5×10^{-2}	Greenhill *et al.*[14]

no particles on the negative side beyond $-0.01\ (\mathrm{GV})^{-1}$. In the absence of anti-nuclei the number of particles expected on the negative side caused by Coulomb scattering is ~0.3. Thus we can put an upper limit to the flux of anti-helium nuclei as $\sim1\%$ of the flux of helium nuclei in the rigidity range of 14–100 GV. If we split the total rigidity range into the bins of 14–30 GV, 30–50 GV and 50–100 GV, the corresponding upper limits are 2%, 2% and 10%. So far no anti-nuclei have been found in primary cosmic rays and only upper limits exist. Our upper limits, together with those obtained by others, are given in Table 1.

R. P. VERMA
T. N. RENGARAJAN
S. N. TANDON
S. V. DAMLE
YASH PAL

Tata Institute of Fundamental Research, Bombay 5

Received September 12, 1972.

1 Cowsik, R., Damle, S. V., Yash Pal, Rengarajan, T. N., Tandon, S. N., Verma, R. P., and Vidwans, P. A., *Acta Physica Scientiarum Hungaricae*, **29**, Suppl. 4, 535 (1970).
2 Damle, S. V., Yash Pal, Rengarajan, T. N., Tandon, S. N., and Verma, R. P., *Proc. Twelfth Internat. Conf. Cosmic Rays* (Hobart, 1971).
3 Daniel, R. R., and Stephens, S. A., *Proc. Ind. Acad. Sci.*, **63**, 275 (1966).
4 Golden, R. L., Adams, J. H., Boykin, W. R., Deney, C. L., Marar, T. M. K., Heckman, H. H., and Lindstrom, P. L., *Proc. Twelfth Internat. Conf. Cosmic Rays* (Hobart, 1971).
5 Anand, K. C., Daniel, R. R., Stephens, S. A., Bhowmik, R., Krishna, C. S., Aditya, P. K., and Puri, R. K., *Proc. Ind. Acad. Sci.*, **67**, 138 (1968).
6 Pinkau, K., Pollvogt, U., Schmidt, W. K. H., and Huggett, R. W., *Acta Physica Scientiarum Hungaricae*, **29**, Suppl. 1, 291 (1970).
7 Grigorov, N. L., Rapoport, I. D., Savenko, I. A., Nesterov, V. E., and Prokhin, V. L., *Proc. Twelfth Internat. Conf. Cosmic Rays* (Hobart, 1971).
8 Buffington, A., Smith, L. H., Smoot, G., Wahlig, M. A., and Alvarez, L. W., *Proc. Twelfth Internat. Conf. Cosmic Rays* (Hobart, 1971).
9 Ryan, M. J., Ormes, J. F., and Balasubrahmanian, V. K., *Phys. Rev. Lett.*, **10**, 985 (1972).
10 Apparao, M. V. K., *Nature*, **215**, 727 (1967).
11 Bogomolov, E. A., Lubyanaya, N. D., and Romanov, V. A., *Proc. Twelfth Internat. Conf. Cosmic Rays* (Hobart, 1971).
12 Evenson, P., and Meyer, P., *Proc. Twelfth Internat. Conf. Cosmic Rays* (Hobart, 1971).
13 Buffington, A., Smith, L. H., Smooth, G. F., Alvarez, L. W., and Wahlig, M. A., *Nature*, **236**, 335 (1972).
14 Greenhill, J. G., Clarke, A. R., and Elliot, H., *Nature*, **230**, 170 (1971).
15 Aizu, H., Fuzimoto, Y. H., Hasegawa, S., Koshiba, M., Mito, I., Nishimura, J., Yokoi, K., and Schein, M., *Phys. Rev.*, **121**, 1206 (1961).

Cretaceous Deep-sea Manganese Nodules on Timor: Implications for Tectonics and Olistostrome Development

PROBABLY the best known occurrence of fossil manganese nodules closely resembling deep-sea nodules of modern oceans are those of western Timor[1]. They occur with micronodules in a red clay similar to recent deep-sea red clays[2]. Their chemistry and physical characters provide the basis for thinking that these nodules, micronodules and the red clay matrix were originally deposited on the deep-sea floor of a Cretaceous ocean[1–4]. Two questions arise: How did this portion of ocean

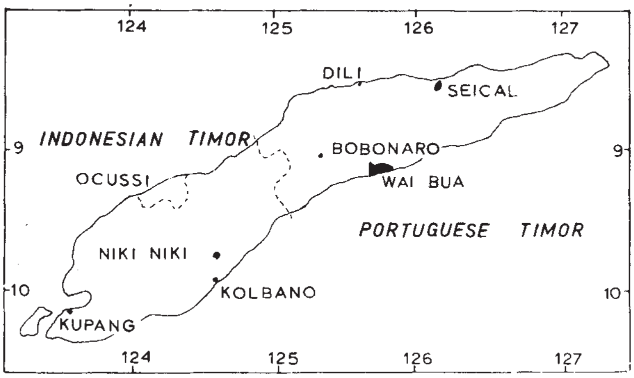

Fig. 1 Location of the Cretaceous ferromanganiferous deposits near Niki Niki and Wai Bua, and the Middle Eocene deposits at Seical.

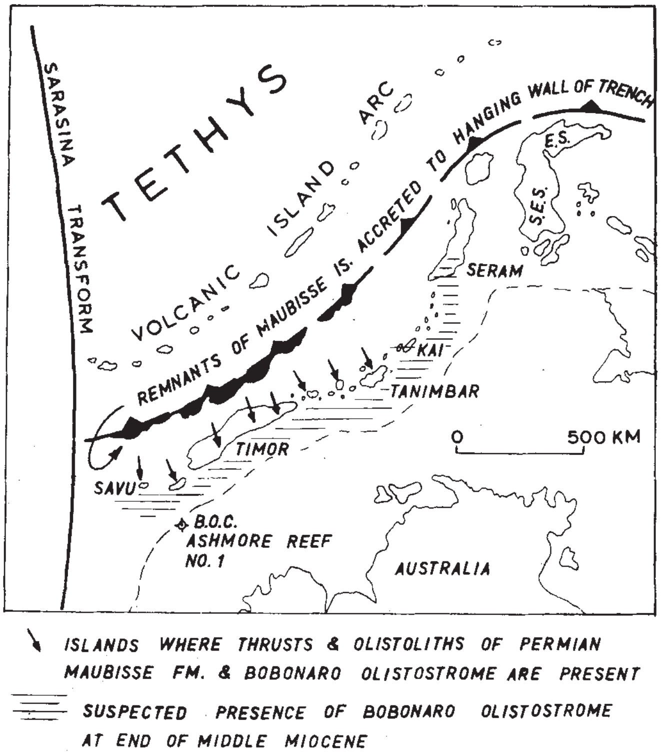

Fig. 2 Reconstruction of the Outer Banda Arc in the Middle Miocene[5] showing the known and inferred emplacement of the Bobonaro Scaly Clay olistostrome. The present distribution of the olistostrome seems to be closely related to the occurrence of overthrust sheets of the Permian Maubisse Formation. The presence of the olistostrome in Kai and Seram is interpreted from reports of mud volcanoes and landslides forming a "soup of shales and limestone blocks"[9]. Its presence below the Timor Trough seems very likely in view of its tendency to thicken southwards in southern Timor, which implies the declivity down which it slid continued southwards towards the Miocene Timor Trough[10].